Materials & Design 213 (2022) 110329

Contents lists available at ScienceDirect

Materials & Design

journal homepage: www.elsevier.com/locate/matdes

A quantitative analysis of dicalcium silicate synthesized via different sol-gel methods

Muhammad Jawad Ahmed [a,*], Katrin Schollbach [a,b], Sieger van der Laan [b], Miruna Florea [a], H.J.H Brouwers [a]

[a] Department of Built Environment, Eindhoven University of Technology, Eindhoven, the Netherlands
[b] Tata Steel RD&T, Ceramics Research Centre, P.O. Box 10000, 1970 CA IJmuiden, the Netherlands

HIGHLIGHTS

- Hiding of CaO and SiO_2 in XRD-amorphous leads to a false impression of the purity.
- Calcium polymer network via the Pechini method yields pure β-dicalcium silicate.
- $CaCO_3$ formation leads to an increase in the calcination temperature.
- The big crystallite size (D_{cryst}) lowers the yield of β-dicalcium silicate.
- The change in Ca/Si stoichiometry from 2.0 to 1.7 is not recommended.

GRAPHICAL ABSTRACT

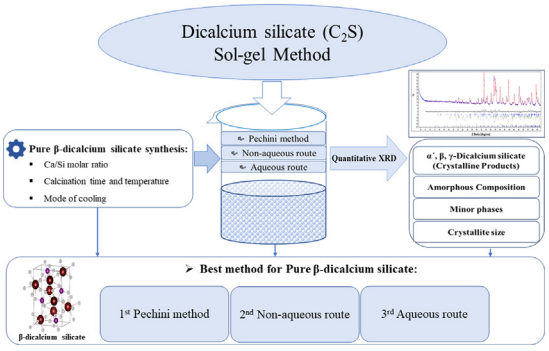

ARTICLE INFO

Article history:
Received 22 August 2021
Revised 16 December 2021
Accepted 16 December 2021
Available online 18 December 2021

Keywords:
Pechini method
Dicalcium silicate
Sol–gel
Polymorphs
Aqueous route
Non-aqueous route
Mean crystallite size

ABSTRACT

In this paper, the synthesis of dicalcium silicate (C_2S) via sol-gel (acid-catalyzed) process including aqueous route, non-aqueous route, and the Pechini method is reported. The composition of C_2S (α, β, and γ) polymorphs, by-products, and amorphous content is established by employing QXRD (quantitative X-ray diffraction) studies. The attention has been focused to comprehend assay-amorphous relationships of C_2S yield. The intermediate dried gels have been investigated via thermal analysis to monitor changes in the gel structures and precursors at low temperatures. The synthetic parameters including calcination time and temperature, Ca/Si molar ratio and mode of cooling have been optimized to get pure β-C_2S with low amorphous content. The dependency of β → γ C_2S polymorphic transformation on mean crystallite size (D_{cryst}) is studied. Overall, the Pechini method exhibits the most promising results for the purity and tuning of β-C_2S polymorph. Moreover, the non-aqueous and aqueous routes require calcining the dried gel at a temperature higher than 1200 ℃ due to the presence of CaO precursors as $CaCO_3$. The theoretical calculations of amorphous content have revealed that the change in the stoichiometry from 2.0 to 1.7 Ca/Si ratio is not a viable solution to improve the C_2S product yield.

1. Introduction

Dicalcium Silicate (C_2S) is an important natural mineral known as larnite or belite. It is a monoclinic (β) polymorph of C_2S and exhibits interesting properties for the non-toxic bioactivity, excellent stability under thermal and chemical conditions, high energy storage capacity as well as flame-resistant [1-3]. It is used in various applications such as white light-emitting diodes (LEDs), high-density energy storage and energy production, environmental remediation, and biomedical engineering [4-7].

* Corresponding author.
E-mail address: m.ahmed@tue.nl (M. Jawad Ahmed).

https://doi.org/10.1016/j.matdes.2021.110329
0264-1275/

C_2S is also a minor component of Portland cement clinker (5–10 wt%) and is becoming more relevant due to the increasing use of alternative binders (belite clinkers contain between 40 and 60 wt% belite mineralogically) [8,9]. It is currently investigated as a solution to reduce the CO_2 emissions of the cement industry as well as supplementary cementitious materials that contain C_2S such as converter steel slag [7,10-12,13]. Therefore, it is important to understand the formation and hydraulic properties of C_2S which is complicated by the existence of five crystalline polymorphs (Fig. 1) [14,15]. The most common modification in the aforementioned materials is β-C_2S and will be the focus of this investigation. The thermodynamically stable polymorph at room temperature is γ-C_2S, which is highly undesirable in Portland cement due to the low hydraulic activity. The transition from α (orthorhombic) to β (monoclinic) is reversible while the transformation from β (monoclinic) to γ (orthorhombic) causes the irreversible disintegration of the beta phase due to microcracks because of a 14 % increase in lattice volume in a phenomenon known as dusting. The C_2S reactivity, in general, depends on the polymorph, foreign ion substitution, and crystallite size. It is possible to stabilize polymorphs other than γ-C_2S at room temperature by the incorporation of dopants such as Al^{3+}, B^{3+}, P^{5+}, S^{6+}, $Fe^{3+,}$ and K^{1+} [16]. The general order of reactivity of different polymorphs of C_2S is as follows [17,18]:

Amorphous C_2S > α-C_2S > β-C_2S > γ-C_2S

C_2S can be synthesized by various traditional (solid-state or fusion) processes and alternatives such as self-combustion or solution combustion synthesis, hydrothermal synthesis, aerosol flame, spray pyrolysis, or the sol–gel process [19,20,21–26]. The sol–gel methods are widely used and based on the gelation of colloidal particles, hydrolysis, polycondensation of nitrates or alkoxides, and hypercritical drying of gel [27]. The resulting product is dried and heated at atmospheric temperature. The sol–gel methods have the advantage of synthesizing β-C_2S that has a high specific surface area (up to 26.5–27 m^2/g^1) and is stable at room temperature without using any additional chemical stabilizers/dopants. The synthesis temperatures also tend to be lower compared to solid-state synthesis [28,22,29,30]. The stability of β-C_2S synthesized via the sol–gel method has been attributed to the small particle size (1–3 μm) that prevents a transformation into γ-C_2S [30].

A qualitative X-ray powder diffraction (XRD) is the standard analytical tool for identifying C_2S polymorphs [31]. However, the diffractograms are typically complex with an overlap of the diffraction peaks of α, β, and γ-C_2S. If the reaction is incomplete other phases such as wollastonite, quartz or free lime can also be present, making analysis even more complex. So, it is often not possible to identify all impurities or C_2S polymorphs, especially if their content is very low. Moreover, the method allows no insight into the amorphous content meaning it is frequently ignored [32]. However, the amorphous C_2S tends to be the most reactive part of the sample, so its content should be known to reliably design materials for various applications.

Quantitative XRD (QXRD, Rietveld method) can solve these problems, especially if an internal standard is applied to determine the amorphous content. It can also be used to derive additional information about a sample, such a crystallite size, which is an important parameter that can determine the stability of C_2S polymorphs. However this method is rarely applied [16,23,27,28,33,34] and to the best of the author's knowledge, not detailed QXRD including amorphous content determination exists of C_2S synthesized via sol–gel (aqueous, non-aqueous, and the Pechini) methods [16,35-37].

Therefore, the aim of this paper is to study the content of C_2S (α′, β, γ) polymorphs quantitatively including amorphous phase and minor phases via three different sol–gel (acid-catalyzed) using the Pechini method, non-aqueous route, and aqueous route. The three methods are compared to see which sol–gel route provides high β-C_2S polymorph yield with low amorphous content [5,38,7]. The different calcination temperatures and durations are compared, as well as changing the Ca/Si stoichiometry [26,39]. The calcination temperatures and times have been chosen to get a clear insight into the relationship between amorphous content, secondary phases, and total C_2S content [16,28,40,41]. The importance of compacting the intermediate dried gel before calcination is shown by comparing loose powder and pressed pellet. The sol–gel reactions such as polyesterification, silica nanoparticle polymerization as well as the transformation of calcium oxide precursors into hydroxide and carbonate are investigated via TG, DTG and DTA analysis. Moreover, the correlation between mean crystallite size (D_{cryst}) and the β to γ-C_2S transformation is investigated.

2. Materials

$Ca(NO_3)_2{\cdot}4H_2O$ (Sigma-Aldrich CAS: 13477–34-4, ≥99.0 %), colloidal SiO_2 (30 wt% Ludox® AM Sigma-Aldrich), colloidal SiO_2 (40 wt% Ludox® AM Sigma-Aldrich), CH_3CO_2H glacial (Sigma-Aldrich CAS: 64–19-7), $Si(OC_2H_5)_4$ (Sigma-Aldrich CAS:78–10-4, ≥99.0), $C_6H_8O_7{\cdot}H_2O$ (VWR, Analytical grade, CAS: 5949–29-1), HNO_3 (Sigma-Aldrich, CAS:7697–37-2, ≥65 %)and C_2H_5OH (Sigma-Aldrich CAS:64–17-5) were used as received. The reagents were added in the stoichiometric ratios corresponding to the synthesis of C_2S unless indicated otherwise.

The molar ratio, calcination temperature, and time, as well as reaction parameters, have been summarized in Table 1 and are based on previously reported synthesis [16,26].

3. Methods

3.1. Pechini method

The $Ca(NO_3)_2{\cdot}4H_2O$ and colloidal silica (40 wt% suspensions in water) were employed as a cation source of Ca and Si at a 2:1 M ratio. The citric acid monohydrate was chosen as a source of α-hydroxy acid to chelate with Ca^{2+}, and ethylene glycol to construct a gel through esterification. The resin content (Rc) was fixed to 85 %, as it gives the best results according to the literature [16]. The Rc can be adjusted with Equation (1);

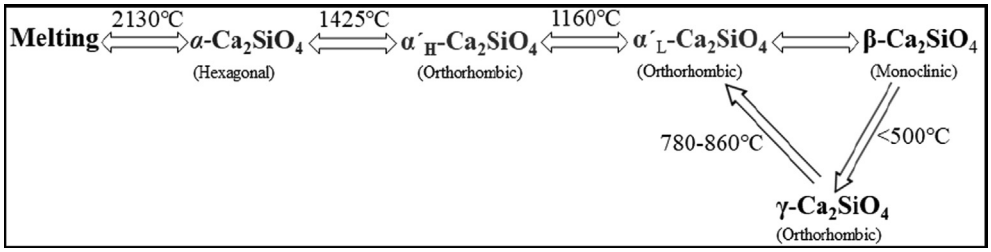

Fig. 1. Different polymorphs of dicalcium silicate (C_2S) and their transition temperatures [11,15].

Table 1
Sol-gel synthesis routes and reaction parameters.

Method	Molar ratio	Reagent	Calcination temperature (℃)	Calcination time (h)	Cooling method
Pechini	2	40 wt% silica sol. (particle size = 20.0–24.0 nm), $Ca(NO_3)_2{\cdot}4H_2O$, 85% resin content	700–1400	1–3	1, 2
Non-aqueous	2	Tetraethyl orthosilicate, $Ca(NO_3)_2{\cdot}4H_2O$, Ethanol	1000–1200	5–8	1
Aqueous	1.7, 2	30 wt% silica sol. (particle size=<150 μm), $Ca(NO_3)_2{\cdot}4H_2O$	1000–1200	5–8	1

1 = cooled in the furnace after switching off the heating (Fig. 2); **2 =** cooled in the furnace followed by a sample is removed at 542℃ and then air-quenched

$$Rc = \langle m_{resin}/(m_{resin} + m_{oxides})\rangle \times 100 \quad (1)$$

m_{oxide} = theoretical yield based on the starting amount of CaO and SiO_2

m_{resin} = the mass of organic precursors.

The $Ca(NO_3)_2{\cdot}4H_2O$ was dissolved in distilled water followed by the addition of citric acid monohydrate. The colloidal silica suspension was added after that already dissolved in ethylene glycol. Then a few drops of nitric acid were added to achieve a pH < 2 to avoid flocculation. The resin content was composed of 60 wt% citric acid monohydrate and 40 wt% ethylene–glycol. The mixture was heated to 80 ℃ to obtain a gel by evaporating water for 6–8 h. Then the gel was charred at 250 ℃ in an oven for 4–5 h. The resultant xerogel was finely ground into powder and calcined at the desired temperature in an alumina crucible at a heating rate of 5 ℃/min. The sample was cooled naturally in a furnace. The rate of furnace cooling showed in Fig. 2. At calcination temperature 1400 ℃, the cooling condition was modified in such a way that one sample was removed from the furnace at 542 ℃ and air-quenched below the aforementioned temperature.

3.2. Non-aqueous method

The TEOS (tetraethyl orthosilicate) and $Ca(NO_3)_2{\cdot}4H_2O$ were employed as a source of Si and Ca respectively with a 1:2 M ratio. The following steps were executed, (1) TEOS was mixed with ethanol (molar ratio C_2H_5OH: TEOS = 1.5) separately. (2) $Ca(NO_3)_2{\cdot}4H_2O$ was dissolved in a minimum amount of ethanol. Then both solutions were mixed followed by the dropwise- addition of glacial acetic acid to reach a pH < 2–3. The sample was left overnight, and a translucent gel was obtained. The gel was dried, ground, pressed into a pellet, and calcined at the desired temperatures using a heating rate of 5 ℃/min [26,30]. The sample was cooled according to Method 1 (Table 1 & Fig. 2).

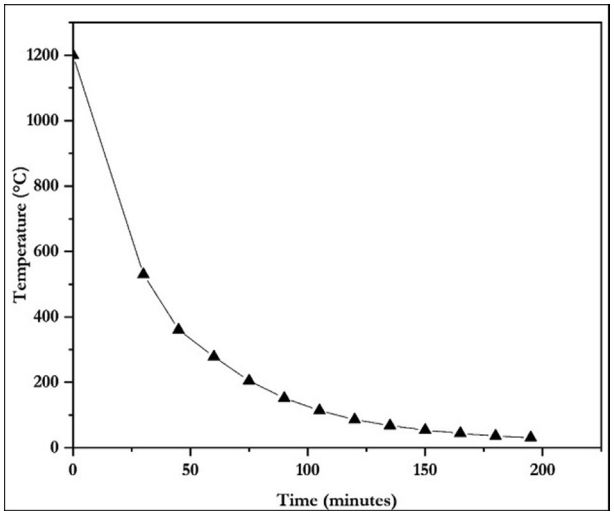

Fig. 2. The rate of furnace cooling employed for sol–gel (acid-catalyzed) synthesis. (cooling Method 1).

3.3. Aqueous method:

The $Ca(NO_3)_2{\cdot}4H_2O$ and colloidal silica (30 wt% suspensions in water) were employed as a source of Ca and Si respectively in a 2:1 M ratio. The $Ca(NO_3)_2{\cdot}4H_2O$ was dissolved in water to complete dissolution followed by the addition of colloidal silica while the solution was stirring. Then a few drops of nitric acid were added to get a pH ≤ 2–3. The sample was heated for 4–6 h at 70 ℃ and a translucent gel was obtained. The gel was stored for 24 h at 38 ℃ in the oven. The gel was then dried, ground, and calcined at the desired temperature with a heating rate of 5 ℃/min. [20,30]. The sample was cooled according to Method 1(Table 1 & Fig. 2).

3.4. Characterization techniques

XRD (X-ray powder diffraction) diffractograms were obtained with a Bruker D2 and D4 (Source: Co K α1 1.7901 Å and K α2 1.7929 Å, Detector: LynxEye). Both instruments have a fixed divergence slit with an opening of 0.5° and 0.04 rad Soller slits. The 2 Theta range was 5° to 90° with a step size of 0.02. All samples for qualitative and quantitative analysis were prepared via back-loading. The synthesized phases were identified with X'Pert Highscore Plus 2.2 employing the ICDD PDF-2 database.

For QXRD (Quantitative X-ray diffraction), an internal standard (Si: 10 wt% of the total sample) was mixed homogenously by using an XRD McCrone micronizing mill. TOPAS 4.2 Bruker software was employed for the quantification and determination of crystallite size using the fundamental peak fitting parameter approach. The crystal structures for quantification were obtained from the ICSD database as shown in Table 2. The error values given in the results are the errors as calculated by TOPAS.

The thermal analysis was done on dried gel samples using a Jupiter STA 49 F1 Netzsch instrument. The sample was heated from 40 ℃ to 1000 ℃ at the rate of 5 ℃/min under air environment.

Table 2
ICSD data code and chemical formulas of crystal structures.

Mineral Phases	Chemical formula	Crystal system/ Notation	ICSD
Dicalcium silicate	Ca_2SiO_4	Orthorhombic/α′	81,097
Dicalcium silicate	Ca_2SiO_4	Monoclinic/β	81,096
Dicalcium silicate	Ca_2SiO_4	Orthorhombic/γ	81,095
Wollastonite	$CaSiO_3$	Triclinic, 1-A	23,567
Wollastonite	$CaSiO_3$	Monoclinic, 2-M	201,538
Pseudowollastonite	$CaSiO_3$	Triclinic, 4-A	26,553
Lime	CaO	Cubic	60,199
Calcium aluminum oxide	$Ca_2Al_2O_5$	Orthorhombic	89,708
Grossular	$Ca_3Al_2(SiO_4)_3$	Cubic	31,082
Cristobalite	SiO_2	Cubic	44,269
Quartz low	SiO_2	Trigonal	41,446

The IR spectra were measured with a Fourier Transform-Infrared spectrometer (FT-IR) from Perkin Elmer Frontier FTIR. The spectrometer was equipped with diffuse reflectance device Gladi. ATR. Sixty scans were acquired with optical retardation of 0.25 cm and a resolution of 4 cm^{-1} from 400 to 4000 cm^{-1}.

Scanning Electron Microscopy (SEM) was performed using a Phenom Pro-X scanning electron microscope. The sample was prepared by spreading the powder on conductive carbon adhesive tapes followed by coating with gold. Micrographs were recorded using a backscattered electron detector (BSE) at 15 kV with a spot of four.

4. Results and discussion

4.1. Results of C_2S synthesis via the Pechini method

The intermediate, amorphous gel produced with the Pechini method was charred at 250 °C, and then TG/DSC was analyzed to determine the lowest calcination temperature C_2S synthesis (Fig. 3(a, b)). The decomposition of the dried gel can be broadly divided into three main steps. The first mas-loss step from 40 to 250 ℃ can be attributed to the loss of water physisorbed on the surface of the dried gel. The second strong exothermic step (250–600 ℃) can be assigned to the resin breakdown and residual carbon combustion. The mass loss step around 251–350 °C can be attributed to the polymer fragmentation, formed by polyesterification of citric acid and ethylene glycol. The mass loss step around 405–445 °C may occur due to the decomposition of the carboxylic group, carbonates, and nitrates. The exothermic peak of polymer fragmentation may overlap with the endothermic process of decomposition of nitrates and carbonates in DTA analysis. The third slight exothermic step (600–700 ℃) is attributed to the crystallization of C_2S. The TG signal becomes stable at around 650 to 700 ℃. So, 700 ℃ was chosen as the lowest calcination temperature [31].

The C_2S synthesized via the Pechini method has been investigated after heating the precursor to temperatures in the range of 700–1400 ℃ and a calcination time of 1–3 h with cooling Method 1 unless stated otherwise. The XRD diffractograms without internal standard (Silicon) are shown in Fig. 4. And the results of QXRD are shown in Table 3.

At 700 ℃, the α′-C_2S (22.5 wt%) polymorph and amorphous content (68.3 wt%) were the major phases with minor amounts of β-C_2S (9.2 wt%) present. The particles calcined at 700℃ appeared spherical, porous, and highly agglomerated (Fig. 8 (a)), which is align with the literature [42].

By increasing the calcination temperature to 800 ℃, the dominant crystalline phase became β-C_2S (27.5 wt%) alongside α′-C_2S (19.4 wt%) and amorphous content (53.1 wt%). The high amorphous content at 700–800 ℃points out that the C_2S (α′ and β) polymorphs matrix is poorly crystalline.

When the calcination temperature was raised to 900 ℃, the α′-C_2S completely transformed to β-C_2S (83.0 wt%). The amount of amorphous content decreased from 53.1 to 16.8 wt% while only β-C_2S crystallized out of the amorphous matrix. A further increase in calcination temperature to 1000 ℃ led to only a small increase in β-C_2S (83.7 wt%). At 1100 ℃, γ-C_2S (2.9 wt%) started to appear, which increased slightly (3.7 wt%) at 1200 ℃. The γ-C_2S formation was observed at a calcination temperature of 1300 ℃ with natural furnace cooling (cooling Method 1) in the earlier studies [37]. Overall, β-C_2S was the dominant product in the range of 900–1200 ℃. The sequence of phase development was consistent with previous studies [36]. Minor amounts of wollastonite, quartz, grossular, and CaNaAlO were observed during the synthesis. The quartz and wollastonite are likely due to incomplete conversion of reactants, while the impurity phases of grossular and CaNaAlO may form due to trace amounts of aluminum and sodium in the reagent or the corundum from the crucible [37].

At 1400 ℃, the amount of γ-C_2S reached 23.4 wt% in the sample cooled via Method 1. The γ-C_2S is not formed at 1400℃, because it is a low-temperature modification. Instead, it is formed out of β-C_2S during cooling. The phenomenon of β → γ-C_2S transformation is dependent upon particle size [41]. With increasing the calcination temperature, the crystallite size of the C_2S increases due to sintering effects. The internal strain is generated inside the β-C_2S crystals during cooling. This strain becomes larger with increasing crystallite size and will result in the transformation of β-C_2S into γ-C_2S, once a critical crystallite size is achieved. The β-destabilization can be restricted by increasing the cooling speed (physical stabilization) above the γ-stability field temperature or by incorporating impurities into the crystal structure (chemical stabilization) [39]. The calcined sample at 1400 °C cooled down via Method 2 decreased γ-C_2S from 23.4 wt% to 5.7 wt% with 92.0 wt% β-C_2S [41]. The metastable β-C_2S achieved at 1400 ℃ with cooling Method 2 was analyzed 8 weeks later and no conversion into γ-C_2S had taken place. The average crystallite size ($D_{crystallite}$) growth at increasing calcination temperature and its correlation with C_2S polymorphic transformation is discussed in Section 4.4.

A few representative FTIR spectra have been taken to investigate bonding systems (Fig. 7 (a)). In the case of the Pechini method, the strong and broadband regions at 896 cm^{-1} and 509 cm^{-1} are attributed to α'_H-C_2S (orthorhombic). The band at 997 cm^{-1} can be attributed to β-C_2S. At 900 ℃ and 1000 ℃, the new bands 503 cm^{-1}, 540 cm^{-1} in the SiO_2-bending region and 847 cm^{-1}, 865 cm^{-1}, 895 cm^{-1}, 992 and 1016 cm^{-1} in the SiO_2-stretching region clearly indicates the presence of β-C_2S. As the calcination temperature is elevated higher than 1000 ℃, a new band appears at 497 cm^{-1} in the SiO_2-bending region indicating the presence of γ-C_2S. The strong band regions at 519 cm^{-1}, 541 cm^{-1}, 841 cm^{-1}, 893, and 991 cm^{-1} indicate the strong presence of β-C_2S. The FTIR studies of C_2S synthesized via the Pechini method exhibited complete agreement with previous studies [43,27,41].

4.2. Results of C_2S synthesis via the non-aqueous route

The thermal events of intermediate gel dried at 150 °C were analyzed via TG and DSC as shown in Fig. 3(c, d). The first endothermic mass loss step occurs due to the loss of physisorbed water on the dried gel sample. The second strong endothermic event is comprised of the three mass loss steps. The mass loss of around 440–535 °C occurs due to the removal of by-products (H_2O and C_2H_5OH) upon completion of TEOS hydrolysis and condensation. The mass loss around 536–584 °C may be assigned to dehydroxylation of portlandite ($Ca(OH)_2$) and decomposition of nitrates. The mass loss around 604–670 °C likely occurs due to the removal of carbon oxide from calcite ($CaCO_3$). The third slight exothermic event with no mass loss is attributed to the phase crystallization out of the amorphous matrix [44]. It is clear from the thermal event analysis that in the first step, the water evaporates to form xerogel, and calcium nitrates precipitate onto the surface of the network. In the next step, the calcium nitrate breaks into the calcium oxide to react with the silica network to form dicalcium silicate. The surface and internal silanol groups may convert into the strained siloxane bridges in thermally induced condensation of hydroxylated silica surface below 500 °C. The strained siloxane bridges are converted into stable siloxane groups at a temperature higher than 500 °C. The presence of calcite around 600–700 °C as a calcium source delays the supply of calcium oxide for the reaction. Moreover, stable siloxane bridges react at a very slower rate than strained siloxane bridges [45]. Conclusively, the presence of calcite as a calcium source requires a high calcination

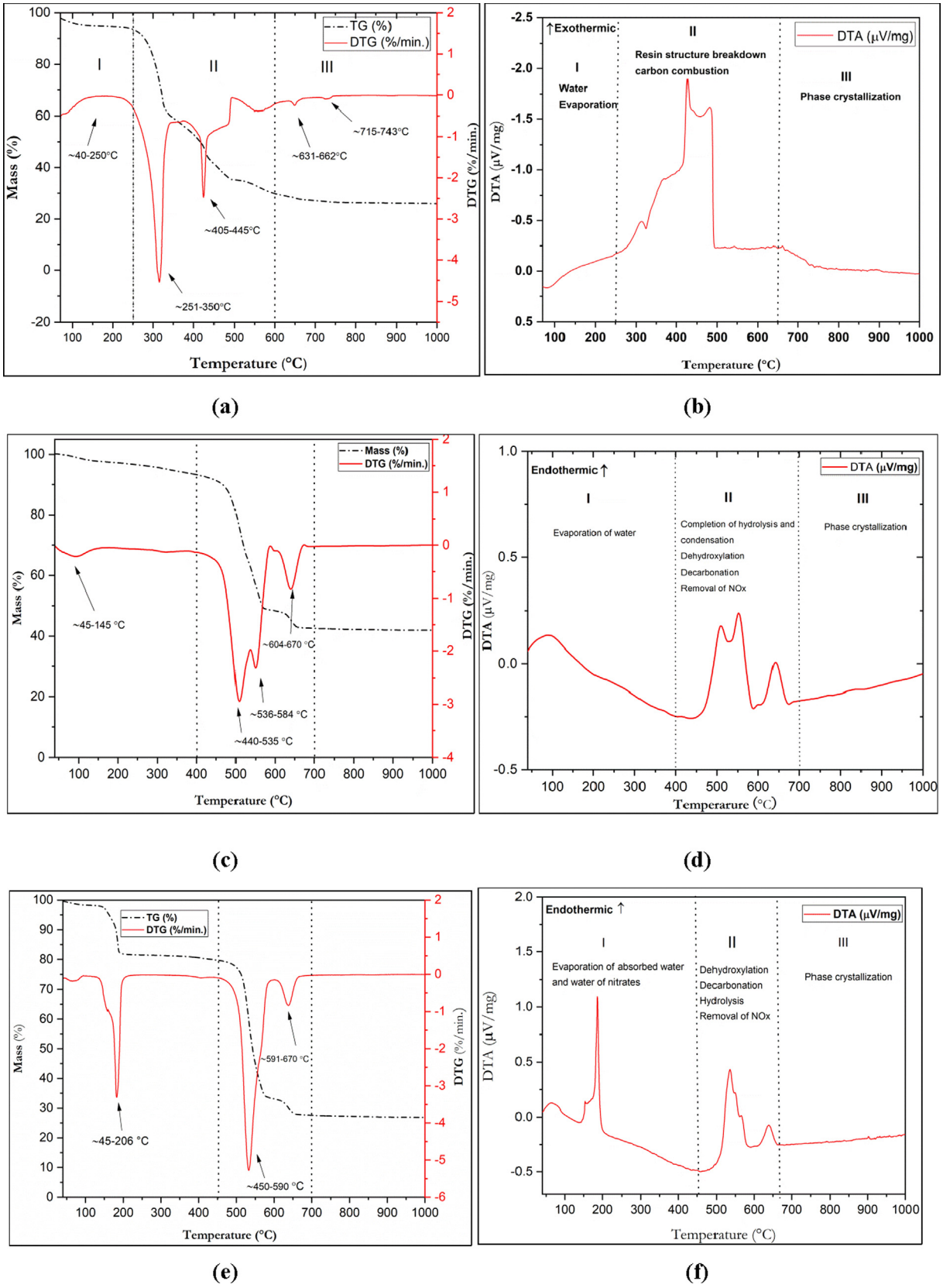

Fig. 3. Thermal analysis of intermediate dried gels from all sol–gel routes (a) TG and DTG (b) DTA analysis of the dried gel synthesized from the Pechini method pre-charred at 250 ℃ (c) TG and DTG (d) DTA analysis of the dried gel synthesized via non-aqueous route and pre-dried at 150 ℃ (e) TG and DTG (f) DTA analysis of the dried gel synthesized via aqueous route and pre-dried at 150 ℃.

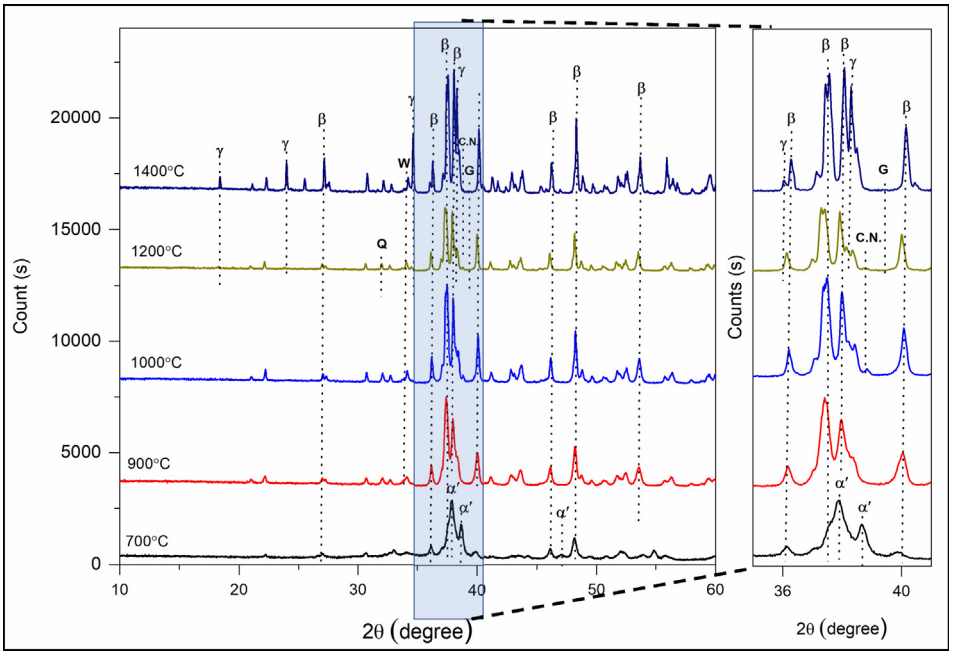

Fig. 4. XRD pattern of the dried gel obtained with the Pechini method after heating to different temperatures. The crystalline phases are labeled as **α'**= α'-C_2S, **β** = β-C_2S, **γ** = γ-C_2S, **W** = wollastonite-2 M, **C.N** = Calcium sodium Aluminum oxide, **G** = grossular, **Q** = quartz.

Table 3
QXRD of the C_2S synthesized via Pechini method with error values.

Temperature (℃)	700	800	900	1000	1100	1200	1400	1400	*1400
Calcination time (h)	**3**	**3**	**1**	**1**	**1**	**1**	**1**	**1**	**1**
Cooling method	**1**	**1**	**1**	**1**	**1**	**1**	**1**	**2**	**2**
α'-C_2S (wt. %)	22.5 ± 0.9	19.4 ± 0.7							
β-C_2S (wt. %)	9.2 ± 0.8	27.5 ± 0.6	83.0 ± 0.2	83.7 ± 0.3	85.2 ± 0.3	86.4 ± 0.3	76.1 ± 0.3	92.4 ± 0.3	92.0 ± 0.3
γ-C_2S (wt. %)					2.9 ± 0.2	3.7 ± 0.2	23.4 ± 0.2	5.7 ± 0.2	6.1 ± 0.2
Wollastonite-2 M (wt. %)			0.2 ± 0.1		0.3 ± 0.2				
Quartz low (wt. %)						0.8 ± 0.1			
Grossular (wt. %)					0.7 ± 0.1	0.6 ± 0.1	0.6 ± 0.1	0.3 ± 0.1	0.4 ± 0.1
CaNaAlO (wt. %)				0.3 ± 0.1		0.4 ± 0.1			
XRD-amorphous (wt. %)	68.3 ± 1.6	53.1 ± 1.0	16.8 ± 1.0	15.9 ± 1.4	10.9 ± 1.3	8.0 ± 1.3		1.6 ± 1.5	1.5 ± 1.4

***1400** = 8 weeks old sample.

temperature for the complete conversion of reactants into a product.

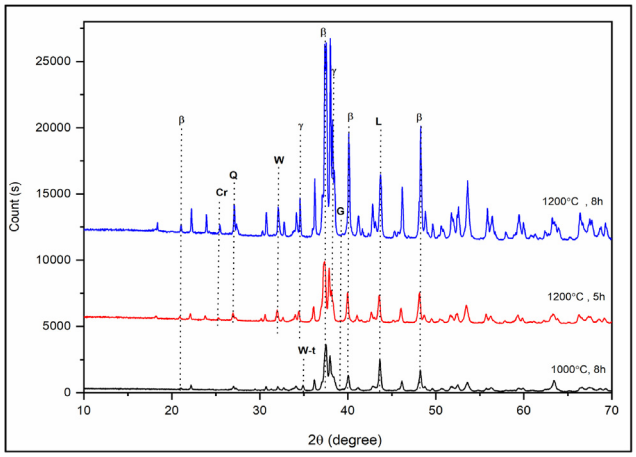

Fig. 5. XRD pattern of C_2S synthesized via non-aqueous route. The crystalline phases are labeled as **β** = β-C_2S, **γ** = γ-C_2S, **W** = wollastonite-2 M, **W-t** = wollastonite-triclinic **L** = lime, **G** = grossular, **Cr** = cristobalite, **Q** = quartz.

For the C_2S synthesis via the non-aqueous route, the precursors were calcined in the temperature range of 1000–1200 ℃ and a calcination time from 5 to 8 h was chosen [30]. The XRD patterns without internal standards are shown in Fig. 5 and the results of QXRD are shown in Table 4.

When the intermediate dried-gel was fired at 1000 ℃ for 8 h, the major phase was β-C_2S (73.4 wt%) with wollastonite (5.1 wt%), unreacted lime (7.6 wt%), and (12.3 wt%) XRD amorphous. An SEM micrograph of C_2S synthesized at 1000 ℃ is shown in Fig. 8 (b) and shows the same morphology reported in other studies [42]. The presence of free-lime and wollastonite indicates that the conversion of reactants was incomplete. Therefore, the calcination temperature was elevated to 1200 ℃ for 5 h, and γ-C_2S (4.5 wt%) appeared alongside β-C_2S (81.3 wt%) with a clear decrease in wollastonite (1.7 wt%) and free-lime (4.9 wt%) as well as a decrease of the amorphous content to 5.7 wt%. A further increase of the calcination time from 5 to 8 h at 1200 °C yielded more γ-C_2S (16.7 wt%) and a decrease in β-C_2S (from 81.3 to 75.1 wt%). The 3.8 wt% of amorphous content at 1200 °C for 8 h calcination suggested that most of the C_2S matrix was crystalline. However, it was successful in further decreasing the lime (2.7 wt%) and wollastonite (0.6 wt %) content. A small amount of quartz and cristobalite was also visible, as the remaining, unreacted SiO_2 in the amorphous content

Table 4
Qxrd of the product synthesized by a non-aqueous route of the sol–gel method with error values.

Temperature (℃)	1000	1200	1200	1200
Calcination time (h)	**8**	**5**	**8**	**5**
Sintered sample morphology	**Pressed pellet**	**Pressed pellet**	**Pressed pellet**	**Powder**
β-C_2S (wt. %)	73.4 ± 0.6	81.3 ± 0.3	75.1 ± 0.3	53.1 ± 0.2
γ-C_2S (wt. %)		4.5 ± 0.2	16.7 ± 0.2	11.1 ± 0.1
Wollastonite-triclinic (wt. %)	5.1 ± 0.7			
Wollastonite-2 M (wt. %)		1.7 ± 0.1	0.6 ± 0.1	0.2 ± 0.1
Pseudo-wollastonite (wt. %)				4.1 ± 0.2
Lime (wt. %)	7.6 ± 0.1	4.9 ± 0.1	2.7 ± 0.1	3.2 ± 0.1
Grossular (wt. %)	0.6 ± 0.2	0.6 ± 0.1	0.1 ± 0.06	1.0 ± 0.1
Quartz (wt. %)		0.2 ± 0.03	0.2 ± 0.03	0.1 ± 0.02
Cristobalite (wt. %)		1.1 ± 0.07	0.8 ± 0.07	
XRD-amorphous (wt. %)	12.9 ± 1.2	5.7 ± 1.5	3.8 ± 1.6	26.8 ± 0.6

started to crystallize. It seems clear that the content of these two phases is only reducing due to sintering reactions taking place at elevated temperatures as well as longer reaction times. Moreover, the wollastonite and lime crystallize directly out of the amorphous phase showing an incomplete reaction. It can be explained based on the thermal events of precursors' transformation during calcination. Firstly, the presence of calcium carbonate during thermal events delays the reaction with the silica network (Fig. 3 (c, d)). Secondly, the formation of Si-O-Si bonds traditionally takes place at high temperatures while the condensation reaction between the –OH group begins at room temperature. However, many of Si-O-Si bonds are not stable even at a temperature higher than 1000 ℃ to achieve bonding energy close to bulk fracture energy [46]. Conclusively, the incomplete polycondensation reaction of Si-O-Si bonding is completed via high-temperature calcination.

An interesting phenomenon was observed when the dried-gel intermediate was calcined in the form of loose powder at 1200 ℃ for 5 as opposed to the standard pellet. The QXRD showed higher XRD-amorphous content (26.8 wt%), γ-C_2S (11.1 wt%) than the pressed pellet results (XRD-amorphous = 3.8 wt%, γ-C_2S = 4.5 wt %). As the energy of the constrained particle is different from the isolated particle. That's why, the pressing of the pellet likely contributes toward the matrix constraint for particle growth and stabilizes more β-C_2S [39]. Considering the results, all the intermediate dried-gel samples synthesized via non-aqueous and aqueous routes are pressed into a pellet before calcination to obtain optimal results.

The transmittance pattern at the 1459–1460 cm^{-1} and 3639 cm^{-1} can be attributed to the calcium carbonates and hydroxide synthesized via the non-aqueous route due to partial carbonation of free lime (Fig. 7 (b)). The bands in the region 992–998 cm^{-1}, 896 cm^{-1}, 840–870 cm^{-1} corresponds to β-C_2S, and the broadening of peaks can be attributed to the formation of γ-C_2S at 1200 ℃ for 8 h calcined sample [30].

4.3. Results of C_2S synthesis via aqueous route

The synthesis of C_2S was also done using the aqueous route of the sol–gel method. The thermal events of intermediate gel dried at 150 °C via aqueous route exhibited the mass loss events such as removal of water of nitrates and physisorbed water followed by the decomposition of nitrates, dehydroxylation of silica network and calcium hydroxide as well as the removal of carbon dioxide from calcium carbonate respectively. (Fig. 3 (e, f)).

The initial Ca/Si molar ratio was 2 and the sample was calcined at 1200℃ for 5 h. The major phase was β-C_2S (77.6 wt%) alongside γ-C_2S (6.6 wt%) and a low amount of XRD-amorphous (3.7 wt%) phase (Table 5). The amount of CaO was rather higher as 9.1 wt% than non-aqueous route (4.9 wt%). Minor phases like quartz (0.1 wt%) and cristobalite (0.8 wt%) were also observed. The high CaO amount indicated an incomplete reaction between the calcium and silica precursors like the non-aqueous synthesis route. However, the lime content was much higher and the amorphous content lower, which seems the point to a problem with the stoichiometry instead (Table 5). To test this hypothesis as well as to avoid unreacted free lime, the Ca/Si ratio from 2.0 to 1.7 was adjusted as reported in a few studies [26,39]. The intermediate dried gel with a 1.7 Ca/Si starting molar ratio was fired at 1000 ℃, 1140 ℃, and 1200 ℃ respectively.

The XRD patterns with the internal standard are shown in Fig. 6 and the results of QXRD are shown in Table 5. At 1000 ℃ the sample was calcined for 8 h and the major phases were β-C_2S (46.1 wt %) and XRD-amorphous phase (41.3 wt%) beside CaO (6.1 wt%) and wollastonite (3.1 wt%). As the temperature was elevated to 1140 ℃ (5 h calcination), the amount of wollastonite decreased to 0.7 wt% while the CaO content increased (7.8 wt%). A further increase of the calcination temperature to 1200 ℃ (5 h calcination) leads to a slight increase in CaO content (8.7 wt%). The comparison of both starting molar ratios (1.7 and 2.0) indicates that there was no significant decrease in the unreacted CaO (from 9.1 to 8.7 wt%) despite the lower CaO content.

The results clearly show that a reduction in the starting CaO content was not successful in reducing the free lime content after calcination. To make sure that the results are not due to an incorrect quantification, the theoretical composition of the amorphous content was calculated via subtracting all the mineral phases determined with QXRD from the bulk composition (Table 6). If the difference is positive that means the QXRD results are at least theoretically possible. This calculation was done for two samples, one with a Ca/Si ratio of 2 and the other with a Ca/Si ratio of 1.7, both calcined at 1200 ℃ for 5 h.

The theoretical composition of the amorphous content for the Ca/Si = 2 sample is CaO = 0.6 mol. % and SiO_2 = 3.5 mol. %, showing that a lot of the SiO_2 remains XRD-amorphous while the CaO tends to crystallize. In the Ca/Si = 1.7 sample, the theoretical composition of the amorphous content is CaO = -1 mol. %, SiO_2 = 4.3 mol. %. The CaO content is negative that is not possible for a real phase. Considering the error of QXRD, it can be assumed that the real CaO content in the amorphous phase is around 0 mol. %, and thus it consists entirely of amorphous SiO_2. Conclusively, the change in stoichiometry (2.0 to 1.7 Ca/Si molar ratio) is not a viable solution to convert more reactants into β-C_2S.

The TG/DSC analysis of the pre-dried intermediate at 150 °C offers an explanation for this phenomenon (Fig. 3(c,d,e,f)). It clearly shows that the formation of calcium carbonate and the incomplete Si-O-Si network are the inherent issues of the aqueous and non-aqueous routes of sol–gel synthesis. Conclusively, the part of the calcium tends to react with the amorphous silica during high-temperature sintering and long calcination time. This explains the gradual decrease of free lime and wollastonite when the

Table 5
QXRD of the product synthesized by aqueous route with error values.

Temperature (℃)	1000	1140	1200	1200
Calcination time (h)	**8**	**5**	**5**	**5**
Ca/Si molar ratio (mol)	**1.7**	**1.7**	**1.7**	**2**
β-C_2S (wt. %)	46.1 ± 0.3	74.3 ± 0.3	78.7 ± 0.3	77.6 ± 0.9
γ-C_2S (wt. %)	2.8 ± 0.2	11.6 ± 0.2	7.8 ± 0.2	6.6 ± 0.3
Lime (wt. %)	6.1 ± 0.2	7.8 ± 0.1	8.7 ± 0.1	9.1 ± 0.2
Grossular (wt. %)	0.5 ± 0.2	1.0 ± 0.2	1.0 ± 0.2	2.0 ± 0.3
Quartz (wt. %)		0.04 ± 0.02	0.04 ± 0.02	0.1 ± 0.05
Cristobalite (wt. %)				0.8 ± 0.2
Wollastonite-2 M (wt. %)		0.7 ± 0.2	0.6 ± 0.2	
Wollastonite-1A (wt. %)	3.1 ± 0.2			
XRD amorphous (wt. %)	41.3 ± 1.2	4.6 ± 1.2	3.2 ± 1.3	3.7 ± 2.3

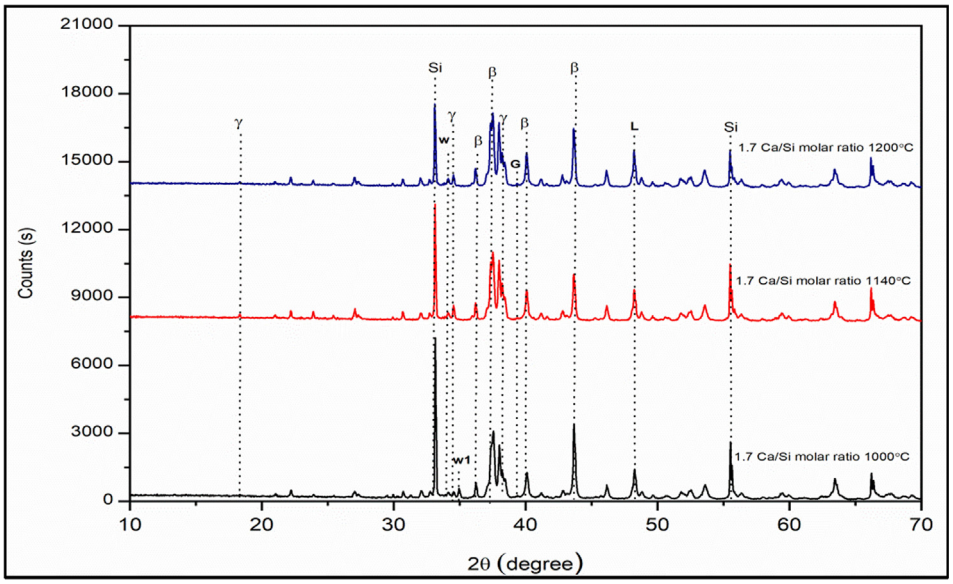

Fig. 6. XRD pattern of C_2S synthesized via an aqueous route of the sol–gel method. The crystalline phases are labeled as **Si** = as internal standard **β** = β-C_2S, **W** = wollastonite-2 M, **L** = lime, **G** = grossular, **γ** = γ-C_2S, **W1** = wollastonite-1A.

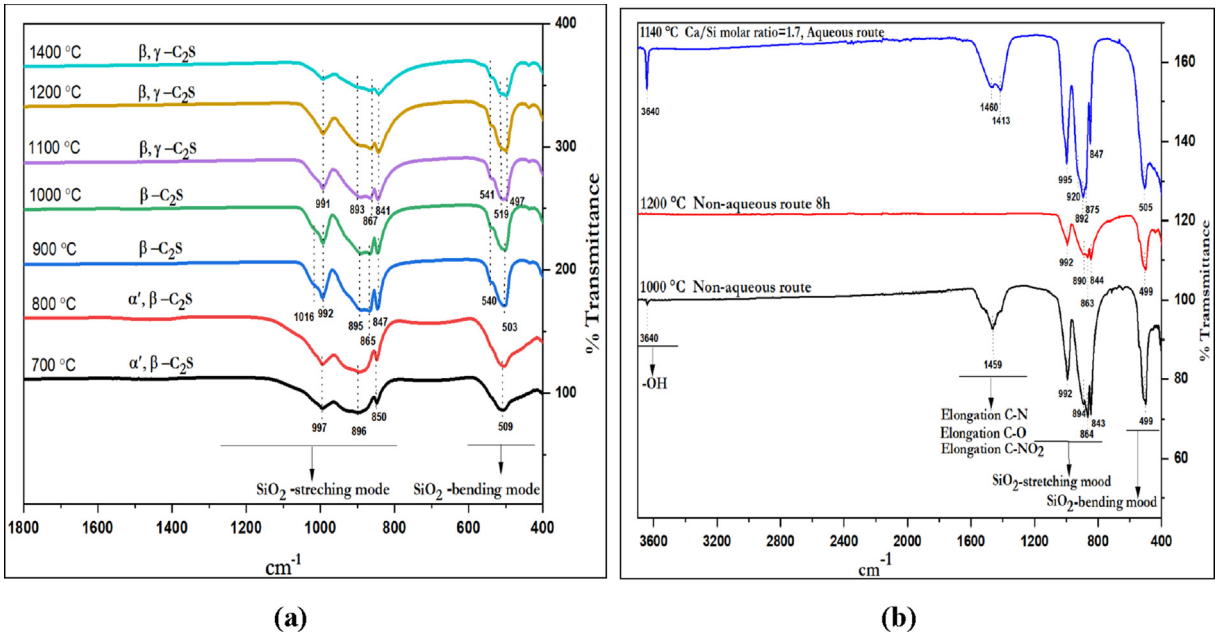

Fig. 7. a) FTIR spectra of C_2S synthesized via Pechini method. **b)** FTIR spectra of C_2S synthesized via non-aqueous and aqueous routes.

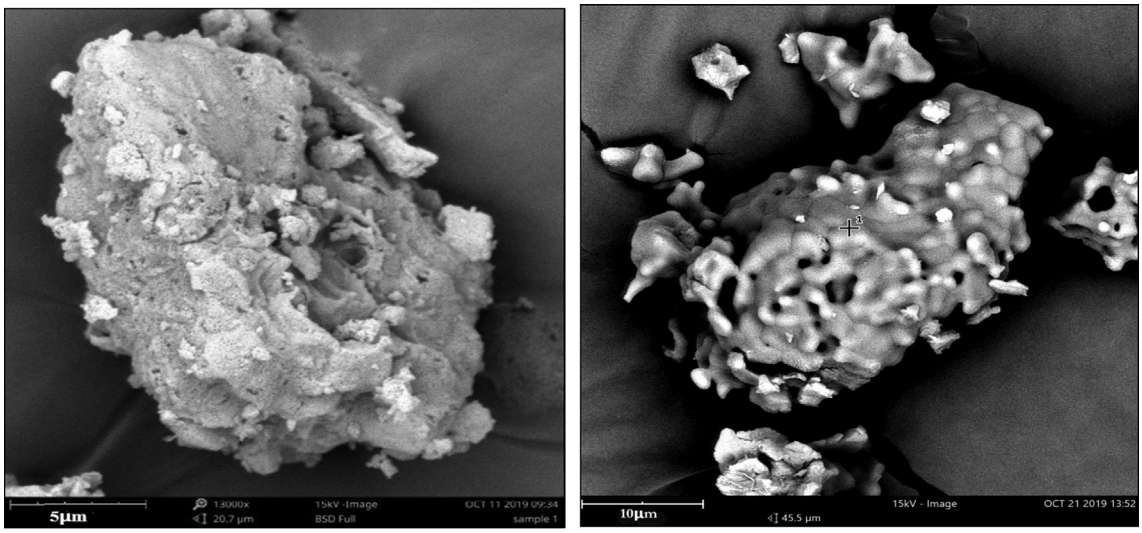

Fig. 8. SEM micrograph of C_2S synthesized via **a)** the Pechini method calcined at 700 ℃ **(b)** non-aqueous route at 1000 ℃.

Table 6
Theoretical amorphous content composition of samples synthesized via the aqueous route. Both samples were sintered at 1200 ℃ for 5 h. The theoretical amorphous oxide composition is the difference between the starting composition and the oxides contained in the crystalline phases.

Ca/Si molar ratio	**2**			**1.7**		
	QXRD (wt. %)	**CaO** (mol. %)	**SiO_2** (mol. %)	**QXRD** (wt. %)	**CaO** (mol. %)	**SiO_2** (mol. %)
Starting Composition		**66.7**	**33.3**		**63**	**37**
Total C_2S	84.2	56.2	28	86.5	54.5	32
Lime	9.1	9.1		8.7	8.7	
Grossular	2	0.9	0.9	1	0.4	0.4
Quartz	0.1		0.1			
Cristobalite	0.8		0.8			
Wollastonite-2 M				0.6	0.4	0.2
Total		**66.2**	**29.8**		**64**	**32.6**
Amorphous	3.7	0.6	3.5	3.2	−1	4.3

calcination temperature is raised from 1000 to 1200 °C (Table 4). Moreover, the alkoxide-assisted Si-O-Si network as in the case of the non-aqueous route tends to react with calcium precursors more efficiently than an aqueous route. (Table 4 and 5)

The FTIR studies of the aqueous route (1.7 Ca/Si molar ratio at 1140 ℃), the broadening of vibration peaks indicated the change in the symmetry order from β (monoclinic) to γ (orthorhombic) showing the presence of γ-C_2S (Fig. 7 (b)). All this information exhibited a compromise with previously reported FTIR studies [41].

4.4. Effect of calcination temperature on C_2S mean crystallite size (D_{cryst}):

The idea of mean crystallite size (D_{cryst}) helps to understand the C_2S polymorphic transformation at varying calcination temperatures because it is the main factor for the stabilization of β-C_2S without any chemical stabilizer [41]. In the case of the Pechini method, the D_{cryst} increases as the calcination temperature are raised from 700 ℃ to 1400 ℃ (Fig. 9).

The D_{cryst} size can be determined for each C_2S polymorph as part of the QXRD and as such is taken directly from TOPAS. At 700–800 ℃, a D_{cryst} size < 27 nm was observed for the α′- C_2S polymorph and would be one of the reasons for the high-temperature polymorph stabilization . From 700 to 1400 ℃, the crystallite size of β-C_2S increases from 27 nm to as big 102 nm in the case of cooling Method

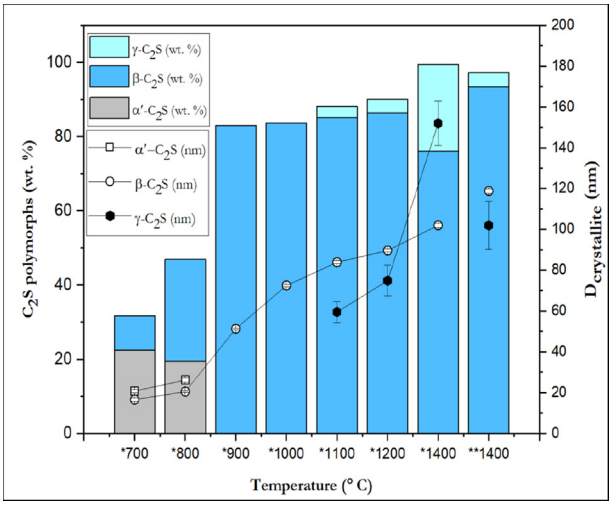

Fig. 9. Correlation between temperature (℃), mean crystallite size D_{cryst} (nm) and polymorphic transition of C_2S (α, β, γ) synthesized by the Pechini method (*=the sample is cooled according to Method 1), (**=the sample is cooled down via Method 2).

1. The γ-C_2S started to appear with a D_{cryst} of about 59 nm alongside β-C_2S 83 nm at 1100 ℃. In the previous studies, the critical particle size 5–10 µm was reported for β-C_2S stabilization [39,41]. In the

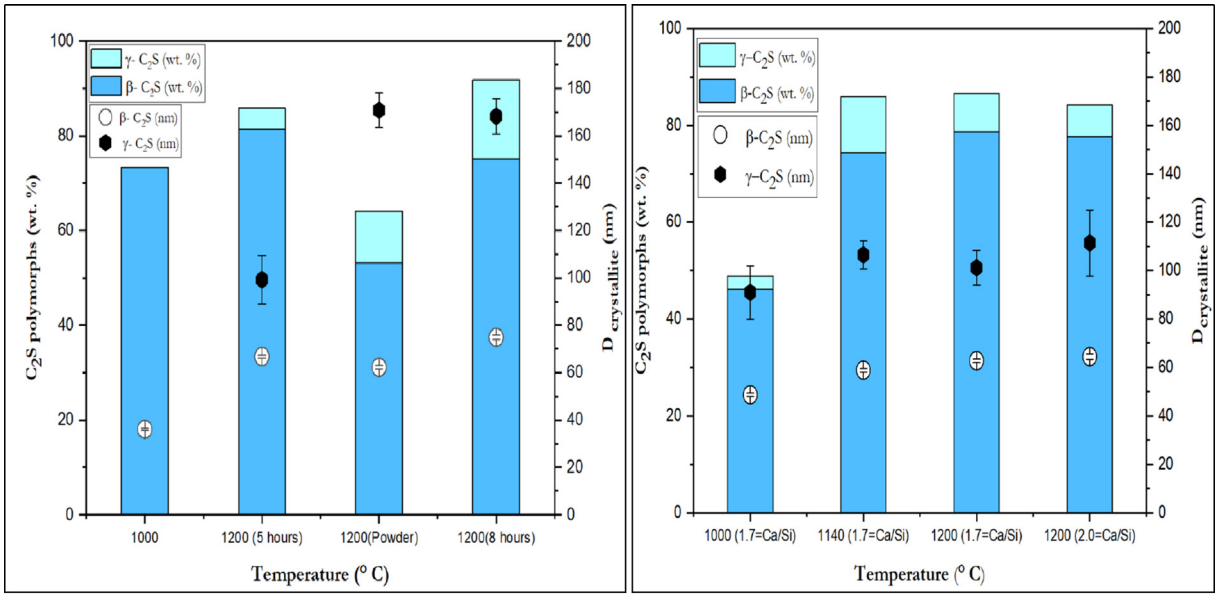

Fig. 10. (**a**) Correlation of calcination temperature with D_{cryst} size (nm) of β and γ-C_2S polymorphs synthesized via non-aqueous route. (**b**) Correlation of calcination temperature with D_{cryst} size (nm) of β and γ-C_2S polymorphs synthesized via aqueous route.

present studies, the D_{cryst} is considered which is much smaller than the reported critical particle size. Therefore, the critical D_{cryst} for β-C_2S stabilization at room temperature seems to be below 83 nm in the case of Pechini synthesis. At 1400 ℃, the D_{cryst} for β-C_2S can grow to a size of 102 nm approximately at which internal strain generated during cooling may induce γ-C_2S formation (23.4 wt%) in a naturally cooled sample in a furnace (cooling Method 1). When the sample was cooled with Method 2 (Pechini method), the resultant β-C_2S D_{cryst} becomes higherthan 102 nm, the D_{cryst} of β-C_2S cooled via Method 1. This observation points out that the facilitated cooling prevents the larger β-C_2S crystal to transform into the γ-C_2S and leads to an increase in the overall mean crystallite size [41].

In the case of the non-aqueous and aqueous route of the sol–gel method (Fig. 10 (a and b)), the calculated D_{cryst} of β and γ-C_2S polymorph lies in the range of 36–78 and 91–170 (min. to the max.) nm respectively. The D_{cryst} also increases with the calcination temperature and time. It can be concluded that the different route (aqueous, non-aqueous, and the Pechini method) of sol–gel synthesis exhibits their own critical mean crystallite size for the β → γ transformation which depends on synthetic route, starting precursors, calcination temperature, and time as well as cooling conditions and matrix composition (Ca to Si molar ratio). The critical D_{cryst} for the β-C_2S stabilization can only be defined in consideration of the aforementioned parameters.

5. Summary and conclusion

The synthesis of C_2S was investigated via the sol–gel (acid-catalyzed) method including the aqueous route, non-aqueous route, and the Pechini method. The C_2S synthesized at 700 and 800℃ via the Pechini method contain α'_H-C_2S (22.5–19.4 wt%) along with a high XRD-amorphous (53.1–68.3 wt%) content. The lowest possible temperature for pure β-C_2S (83.0 wt%, 16.8 wt% amorphous content) synthesis in the present study was 900 ℃. Moreover, a small amount of γ-C_2S started to appear at 1100 ℃, and a sudden increase happened at 1400 ℃ due to an increase in the mean crystallite size. However, the adjustment of cooling conditions such as air-quenching of the sample at 542 ℃ (cooling Method 2) reduced the γ-C_2S amount from 23.4 wt% to 5.7 wt% at 1400 ℃. The Pechini method was found to be the best method for pure C_2S synthesis at low calcination temperature. This can easily be attributed to the efficient calcium polymer network as an intermediate, avoiding the formation of calcium hydroxide and calcium carbonate that only tends to react with the silica network at high temperatures. The non-aqueous route of the sol–gel method exhibited the second most promising results to synthesize a high amount of β-C_2S (81.3 wt%) with low lime (2.7 wt%) and amorphous (3.8 wt%) content at 1200 ℃ calcined for 5 h. The product calcined at 1000 ℃ always contains wollastonite and unreacted lime. The insight about by-products such as quartz, cristobalite, wollastonite, and lime can easily be overlooked via standard XRD analysis due to high peak overlapping. The presence of these phases is due to the formation of calcium carbonate and amorphous silica during calcination leads to an inherent problem of the non-aqueous route. The only mitigation strategy is to calcine the samples at high temperatures for a long time. This strategy would negate the advantage of sol–gel synthesis to some extent and stabilize γ-C_2S due to the large mean crystallite size. Moreover, the pressing of intermediate dried gel into pellet is recommended for high β-C_2S yield and low amorphous content. Comparatively, the aqueous route of a sol–gel method was found to be the least promising method of sol–gel synthesis. The lack of alkoxide assisted Si-O-Si efficient network and formation of calcium carbonate promotes the high amount of unreacted CaO and silica phases. The calculation of QXRD and theoretical composition of amorphous content concluded that any change in the stoichiometry of Ca and Si precursors lower than 2 would lead to the unreacted silica and calcium oxide hiding as XRD amorphous content rather than facilitation of pure β-C_2S synthesis. That's why the change in stoichiometry is not recommended. It has been observed that the D_{cryst} (mean crystallite size) for β → γ transformation depends on the thermal history (calcination temperature and time, mode of cooling), route of sol–gel (Pechini, non-aqueous and aqueous) synthesis, and matrix (calcium or silica-rich) composition. Considering

all these parameters, the critical D_{cryst} for β-C_2S stabilization was recorded below 83 nm approximately in the case of Pechini method synthesis.

In summary, the present work provides a detailed understanding of the advantages and disadvantages of the different sol–gel methods. This study shows the importance of considering the amorphous content, as it can mask impurities/secondary phases in the synthesized samples. This knowledge can be used for reliably designing and understanding the C_2S based materials for electronics, biomedical engineering, and building materials applications.

Data availability statement:

The raw/processed data required to reproduce these findings cannot be shared at this time due to technical limitations.

Declaration of Competing Interest

The authors declare that they have no known competing financial interests or personal relationships that could have appeared to influence the work reported in this paper.

Acknowledgment

The authors would like to acknowledge the financial support by NWO (The Netherlands Organisation for Scientific Research) for funding this research (project no.10023338) and M2i (Materials Innovation Institute) for managing this project. Furthermore, the authors wish to express their gratitude to the following sponsors of this research: Tata Steel; ENCI; V.d. Bosch Beton; Beton Mortel; Inashco; Hess.

References

[1] L. Mohammed, H.G. Gomaa, D. Ragab, J. Zhu, Magnetic nanoparticles for environmental and biomedical applications: A review, Particuology. 30 (2017) 1–14, https://doi.org/10.1016/j.partic.2016.06.001.
[2] A.K. Chatterjee, High belite cements—Present status and future technological options: Part I, Cem. Concr. Res. 26 (8) (1996) 1213–1225, https://doi.org/10.1016/0008-8846(96)00099-3.
[3] Z. Gou, J. Chang, Synthesis and in vitro bioactivity of dicalcium silicate powders, J. Eur. Ceram. Soc. 24 (1) (2004) 93–99, https://doi.org/10.1016/S0955-2219(03)00320-0.
[4] O. Shtepenko, C. Hills, A. Brough, M. Thomas, The effect of carbon dioxide on β-dicalcium silicate and Portland cement, Chem. Eng. J. 118 (1-2) (2006) 107–118, https://doi.org/10.1016/j.cej.2006.02.005.
[5] M.S. Upendra Rao, C. Hanumantharayappa, K.P. Ramesh, D. Haranath, Effect of alkali charge compensator on luminescent properties in Eu3+ doped β-dicalcium silicate, Optik (Stuttg) 178 (2019) 1255–1263, https://doi.org/10.1016/j.ijleo.2018.10.015.
[6] M.C. Gather, A. Köhnen, K. Meerholz, White organic light-emitting diodes, Adv. Mater. 23 (2) (2011) 233–248, https://doi.org/10.1002/adma.201002636.
[7] A. Cuesta, A. Ayuela, M.A.G. Aranda, Belite cements and their activation, Cem. Concr. Res. 140 (2021) 106319, https://doi.org/10.1016/j.cemconres.2020.106319.
[8] M.A.G. Aranda, Recent studies of cements and concretes by synchrotron radiation crystallographic and cognate methods, Crystallogr. Rev. 22 (3) (2016) 150–196, https://doi.org/10.1080/0889311X.2015.1070260.
[9] X. Liu, W. Lin, B. Chen, F. Zhang, P. Zhao, A. Parsons, C. Rau, I. Robinson, Coherent diffraction study of calcite crystallization during the hydration of tricalcium silicate, Mater. Des. 157 (2018) 251–257, https://doi.org/10.1016/j.matdes.2018.07.031.
[10] A. van Zomeren, S.R. van der Laan, H.B.A. Kobesen, W.J.J. Huijgen, R.N.J. Comans, Changes in mineralogical and leaching properties of converter steel slag resulting from accelerated carbonation at low CO 2 pressure, Waste Manag. 31 (11) (2011) 2236–2244, https://doi.org/10.1016/j.wasman.2011.05.022.
[11] H.-M. Ludwig, W. Zhang, Research review of cement clinker chemistry, Cem. Concr. Res. 78 (2015) 24–37, https://doi.org/10.1016/j.cemconres.2015.05.018.
[12] J. Skibsted, R. Snellings, Reactivity of supplementary cementitious materials (SCMs) in cement blends, Cem. Concr. Res. 124 (2019) 105799, https://doi.org/10.1016/j.cemconres.2019.105799.
[13] A. Santamaría, A. Orbe, M.M. Losañez, M. Skaf, V. Ortega-Lopez, J.J. González, Self-compacting concrete incorporating electric arc-furnace steelmaking slag as aggregate, Mater. Des. 115 (2017) 179–193, https://doi.org/10.1016/j.matdes.2016.11.048.
[14] T. Staněk, P. Sulovský, Active low-energy belite cement, Cem. Concr. Res. 68 (2015) 203–210, https://doi.org/10.1016/j.cemconres.2014.11.004.
[15] P. Guo, B.u. Wang, M. Bauchy, G. Sant, Misfit Stresses Caused by Atomic Size Mismatch: The Origin of Doping-Induced Destabilization of Dicalcium Silicate, Cryst. Growth Des. 16 (6) (2016) 3124–3132, https://doi.org/10.1021/acs.cgd.5b0174010.1021/acs.cgd.5b01740.s001.
[16] Y.-M. Kim, S.-H. Hong, Influence of minor ions on the stability and hydration rates of β-dicalcium silicate, J. Am. Ceram. Soc. 87 (5) (2004) 900–905, https://doi.org/10.1111/j.1551-2916.2004.00900.x.
[17] L. Nicoleau, A. Nonat, D. Perrey, The di- and tricalcium silicate dissolutions, Cem. Concr. Res. 47 (2013) 14–30, https://doi.org/10.1016/j.cemconres.2013.01.017.
[18] A. Wesselsky, O.M. Jensen, Synthesis of pure Portland cement phases, Cem. Concr. Res. (2009), https://doi.org/10.1007/s11368-012-0598-6.
[19] F.A. Rodrigues, Synthesis of chemically and structurally modified dicalcium silicate, Cem. Concr. Res. 33 (6) (2003) 823–827, https://doi.org/10.1016/S0008-8846(02)01065-7.
[20] L.L. Hench, J.K. West, The sol-gel process - Chemical Reviews (ACS Publications), Chem. Rev. 90 (1) (1990) 33–72.
[21] A.C. Tas, Chemical Preparation of the Binary Compounds in the Calcia-Alumina System by Self-Propagating Combustion Synthesis, J. Am. Ceram. Soc. 81 (11) (1998) 2853–2863, https://doi.org/10.1111/j.1151-2916.1998.tb02706.x.
[22] J.C. Restrepo, A. Chavarriaga, O.J. Restrepo, J.I. Tobón, Synthesis of hydraulically active calcium silicates produced by combustion methods, Mater. Res. Soc. Symp. Proc. 1768 (2015), https://doi.org/10.1557/opl.2015.321.
[23] X.-H. Huang, J. Chang, Low-temperature synthesis of nanocrystalline β-dicalcium silicate with high specific surface area, J. Nanoparticle Res. 9 (6) (2007) 1195–1200, https://doi.org/10.1007/s11051-006-9202-6.
[24] M. Georgescu, J. Tipan, A. Badanoiu, D. Crisan, I. Dragan, Highly reactive dicalcium silicate synthesized by hydrothermal processing, Cem. Concr. Compos. (2000), https://doi.org/10.1016/S0958-9465(00)00017-2.
[25] S.E. Pratsinis, Flame aerosol synthesis of ceramic powders, Prog. Energy Combust. Sci. 24 (3) (1998) 197–219, https://doi.org/10.1016/S0360-1285(97)00028-2.
[26] Y. Tan, Y. Liu, Z. Zhang, M. Hofmann, L. Grover, Comparing three methods for the synthesis of pure ß-dicalcium silicate, in: 2010 4th Int. Conf. Bioinforma. Biomed. Eng. ICBBE 2010, 2010. doi:10.1109/ICBBE.2010.5515290.
[27] A. Meiszterics, L. Rosta, H. Peterlik, J. Rohonczy, S. Kubuki, P. Henits, K. Sinkó, Structural Characterization of Gel-Derived Calcium Silicate Systems, J. Phys. Chem. A. 114 (38) (2010) 10403–10411, https://doi.org/10.1021/jp1053502.
[28] J.J. Thomas, S. Ghazizadeh, E. Masoero, Kinetic mechanisms and activation energies for hydration of standard and highly reactive forms of β-dicalcium silicate (C2S), Cem. Concr. Res. 100 (2017) 322–328, https://doi.org/10.1016/j.cemconres.2017.06.001.
[29] L. Dimesso, Pechini Processes: An Alternate Approach of the Sol-Gel Method, Preparation, Properties, in: and Applications, in: Handb. Sol-Gel Sci. Technol, Springer International Publishing, Cham, 2016, pp. 1–22, https://doi.org/10.1007/978-3-319-19454-7_123-1.
[30] R. Chrysafi, T.h. Perraki, G. Kakali, Sol–gel preparation of 2CaO·SiO2, J. Eur. Ceram. Soc. 27 (2-3) (2007) 1707–1710, https://doi.org/10.1016/j.jeurceramsoc.2006.05.004.
[31] Y. El Khessaimi, Y. El Hafiane, A. Smith, Ye'elimite synthesis by chemical routes, J. Eur. Ceram. Soc. 39 (4) (2019) 1683–1695, https://doi.org/10.1016/j.jeurceramsoc.2018.10.025.
[32] X. Lu, S. Wang, S. Liu, P. Du, Z. Ye, X. Geng, X. Cheng, Phase Identification of γ-And β-Ca2SiO4 via the Rear-Earth Fluorescence Probe, J. Phys. Chem. C. 123 (22) (2019) 13877–13884, https://doi.org/10.1021/acs.jpcc.9b0226210.1021/acs.jpcc.9b02262.s001.
[33] D. Stephan, P. Wilhelm, Synthesis of pure cementitious phases by sol-gel process as precursor, Zeitschrift Fur Anorg. Und Allg, Chemie. 630 (10) (2004) 1477–1483, https://doi.org/10.1002/zaac.200400090.
[34] J. Li, G. Geng, W. Zhang, Y.-S. Yu, D.A. Shapiro, P.J.M. Monteiro, The Hydration of β- and α′ H -Dicalcium Silicates: An X-ray Spectromicroscopic Study, ACS Sustain. Chem. Eng. 7 (2) (2019) 2316–2326, https://doi.org/10.1021/acssuschemeng.8b0506010.1021/acssuschemeng.8b05060.s001.
[35] S.N. Ghosh, P.B. Rao, A.K. Paul, K. Raina, The chemistry of dicalcium silicate mineral, J. Mater. Sci. 14 (7) (1979) 1554–1566, https://doi.org/10.1007/BF00569274.
[36] S.-H. Hong, J.F. Young, Hydration kinetics and phase stability of dicalcium silicate synthesized by the Pechini process, J. Am. Ceram. Soc. 82 (7) (1999) 1681–1686, https://doi.org/10.1111/j.1151-2916.1999.tb01986.x.
[37] I. Nettleship, J.L. Shull, W.M. Kriven, Chemical preparation and phase stability of Ca2SiO4 and Sr2SiO4 powders, J. Eur. Ceram. Soc. 11 (4) (1993) 291–298, https://doi.org/10.1016/0955-2219(93)90028-P.
[38] Q. Sun, J.W. Gustin, F.-C. Tian, S.J. Sidow, B.E. Bergeron, J.-Z. Ma, F.R. Tay, Effects of pre-mixed hydraulic calcium silicate putties on osteogenic differentiation of human dental pulp stem cells in vitro, J. Dent. 108 (2021) 103653, https://doi.org/10.1016/j.jdent.2021.103653.
[39] C.J. Chan, W.M. Kriven, J.F. Young, Physical Stabilization of the β→γ Transformation in Dicalcium Silicate, J. Am. Ceram. Soc. 75 (1992) 1621–1627, https://doi.org/10.1111/j.1151-2916.1992.tb04234.x.

[40] G. Laudisio, F. Branda, Sol-gel synthesis and crystallisation of 3CaO·2SiO2glassy powders, Thermochim. Acta. 370 (1-2) (2001) 119–124, https://doi.org/10.1016/S0040-6031(00)00786-3.
[41] S. Saidani, A. Smith, Y. El Hafiane, L., Ben Tahar, Re-examination of the β→γ transformation of Ca 2 SiO 4, J. Eur. Ceram. Soc. 38 (2018) 4756–4767, https://doi.org/10.1016/j.jeurceramsoc.2018.06.011.
[42] S.H. Hong, J.F. Young, Hydration kinetics and phase stability of dicalcium silicate synthesized by the Pechini process, J. Am. Ceram. Soc. 82 (1999) 1681–1686, https://doi.org/10.1111/j.1151-2916.1999.tb01986.x.
[43] F. Puertas, F. Triviño, Examinations by infra-red spectroscopy for the polymorphs of dicalcium silicate, Cem. Concr. Res. 15 (1) (1985) 127–133, https://doi.org/10.1016/0008-8846(85)90017-1.
[44] Q.T. Phung, N. Maes, S. Seetharam, Pitfalls in the use and interpretation of TGA and MIP techniques for Ca-leached cementitious materials, Mater. Des. 182 (2019) 108041, https://doi.org/10.1016/j.matdes.2019.108041.
[45] R.K. Iler, The Colloid Chemistry of Silica and Silicates, Soil Sci. 80 (1) (1955) 86, https://doi.org/10.1097/00010694-195507000-00014.
[46] C.J. Barbé, D.J. Cassidy, G. Triani, B.A. Latella, D.R.G. Mitchell, K.S. Finnie, J.R. Bartlett, J.L. Woolfrey, G.A. Collins, Sol-gel bonding of silicon wafers: Part 2. Influence of the sol-gel chemistry on bond morphology and interfacial energy, Thin Solid Films. 488 (1-2) (2005) 160–166.